

A New Poly-Si TFTs DC Model for Device Characterization and Circuit Simulation*

Deng Wanling[†], Zheng Xueren, and Chen Rongsheng

(Institute of Microelectronics, South China University of Technology, Guangzhou 510640, China)

Abstract: A new physical current-voltage model for polysilicon thin-film transistors (poly-Si TFTs) is presented. Taking the V-shaped exponential distribution of trap states density into consideration, explicit calculation of surface potential is derived using the Lambert W function, which greatly improves computational efficiency and is critical in circuit simulation. Based on the exponential density of trap states and the calculated surface potential, the drain current characteristics of the subthreshold and the strong inversion region are predicted. A complete and unique drain current expression, including kink effect, is deduced. The model and the experimental data agree well over a wide range of channel lengths and operational regions.

Key words: polysilicon thin film transistors; surface potential; DC model; kink effect

EEACC: 2560B **PACC:** 7340N

CLC number: TN321 **Document code:** A **Article ID:** 0253-4177(2007)12-1916-08

1 Introduction

Polysilicon thin-film transistors (poly-Si TFTs) are becoming more attractive for active-matrix liquid-crystal displays (AMLCD). As a result, physical poly-Si TFTs models suitable for circuit simulation are needed by the electronics industry.

Some existing models for poly-Si TFTs are either too complicated^[1] or incomplete^[2]. Several models^[3-5] for circuit simulators have been built on bulk MOSFETs or SOI models with slight modifications. However, these models are far from satisfactory, as they cannot cope with effects caused by the high density of localized states in the polysilicon bandgap.

Many publications state that the electrical properties of poly-Si TFTs are controlled by defects within the grain boundaries. Werner and Peisl^[6] used conductivity and admittance spectroscopy measurements to obtain a continuous density of states (DOS) at grain boundaries dominated by V-shaped exponential band tails. A similar result was obtained by Fortunato and Migliorato^[7] with a U-shaped DOS distribution. To account for the localized states contribution, a number of mod-

els^[2,8] rely on simplified assumptions, such as the use of a single effective trap energy level, thereby making the models inaccurate, especially in the subthreshold region. Although a few authors^[9,10] considered the exponential DOS distribution, when deriving current-voltage characteristics they needed numerical approaches to calculate surface potential. Iterative numerical calculation of surface potential slows down simulations, which is inappropriate when simulating circuits.

Few authors have analytically solved surface potential and used it to describe the DC characteristics when considering a V-shaped DOS distribution in poly-Si TFTs. It is achieved in this paper.

2 Strong inversion characteristics

In our model, we assume traps to be uniformly distributed over the entire volume of the film. This simplified assumption is available for small grains TFTs^[3,9,10]. In addition, we also assume there is an n-type poly-Si TFT with a gate length L and a gate width W .

Since the polysilicon used for TFTs is either undoped or lightly doped^[11], in the direction of the substrate, the Poisson's equation is^[3,9]

* Project supported by the Cadence Design Systems, Inc.

[†] Corresponding author. Email: dwanl@126.com

Received 21 July 2007, revised manuscript received 30 August 2007

$$\frac{d^2\Psi}{dx^2} = \frac{q}{\epsilon_{si}}(n + N_{TA}^-) \quad (1)$$

where Ψ is the electrostatic potential. If energy zero point is at midgap, the free charge density n is given by

$$n = n_i \exp\left(\frac{\Psi - \phi_n + E_{F0}/q}{\phi_t}\right) \quad (2)$$

where ϕ_n is the channel potential, E_{F0} is the Fermi level in the neutral polysilicon film, and the other parameters have their usual physical meanings.

Since a single exponential DOS distribution in the upper half of the gap (also called a V-shaped DOS distribution)^[6] is assumed, the density of localized ionized acceptor-like traps is given by^[3]

$$N_{TA}^- = g_{cl} \frac{\pi kT}{\sin(\frac{\pi kT}{E_1})} \exp\left(\frac{E_{F0} + q\Psi - q\phi_n - E_C}{E_1}\right) \quad (3)$$

where g_{cl} is the states density, E_1 is the inverse slope of states, and E_C is the energy at the bottom of the conduction band.

For positive values of Ψ , using the relation $\left(\frac{\partial\Psi}{\partial x}\right)_{x=0}^2 = 2\int_0^{\Psi_s} \frac{\partial^2\Psi}{\partial x^2} d\Psi$ and Gauss's law $V_g - V_{fb} - \Psi_s = \frac{\epsilon_{si}}{C_{OX}} \times \frac{d\Psi}{dx}\bigg|_{x=0}$, the implicit relation between gate voltage V_g and surface potential Ψ_s is obtained by

$$V_g - V_{fb} - \Psi_s = \frac{\sqrt{2q\epsilon_{si}}}{C_{OX}} \left\{ n_0 \phi_t \left[\exp\left(\frac{\Psi_s}{\phi_t}\right) - 1 \right] + N_{TA0} \frac{E_1}{q} \left[\exp\left(\frac{\Psi_s}{E_1/q}\right) - 1 \right] \right\}^{1/2} \quad (4)$$

where $n_0 = n_i \exp\left(\frac{-\phi_n + E_{F0}/q}{\phi_t}\right)$ and $N_{TA0} = g_{cl} \times \frac{\pi kT}{\sin(\pi kT/E_1)} \exp\left(\frac{E_{F0} - q\phi_n - E_C}{E_1}\right)$.

Equation (4) cannot be solved in closed form. In general, a distinction can be made between two different operation regions, namely the subthreshold region and the strong inversion region. In the subthreshold region, the Fermi level is close to the midgap, and the localized trapped charge has a much larger concentration than the free electron charge. Therefore, the trapped charge contribution is the most relevant in the subthreshold region. Analogous consideration applies to the strong inversion region, where the Fermi level moves towards the conduction band and the concentration of free charge is much larger than that of the trapped states. Accordingly,

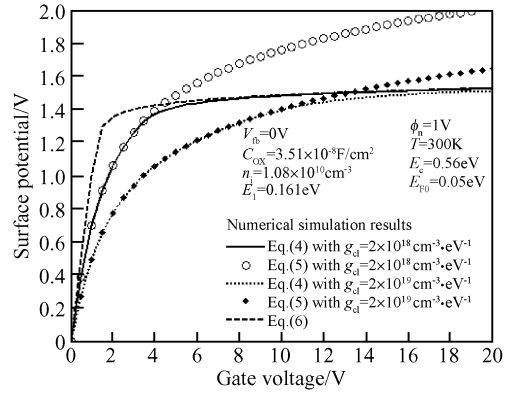


Fig.1 Surface potential as a function of gate voltage obtained from implicit relation Eq. (4) with different g_{cl} . The results of the subthreshold and strong inversion asymptotic approximations, Equations (5) and (6), are also shown.

two asymptotic equations, Equations (5) and (6), can be derived from Eq. (4). In the subthreshold region, the dominant term on the right hand side (RHS) of Eq. (1) is the density of ionized traps N_{TA}^- and the n term is negligible. Therefore, we have

$$V_g - V_{fb} - \Psi_s = \frac{\sqrt{2q\epsilon_{si}}}{C_{OX}} \sqrt{N_{TA0} \frac{E_1}{q} \left[\exp\left(\frac{\Psi_s}{E_1/q}\right) - 1 \right]} \quad (5)$$

In the strong inversion region, the dominant term on the RHS of Eq. (1) is the free charge density n and the N_{TA}^- term is negligible. Therefore, we obtain

$$V_g - V_{fb} - \Psi_s = \frac{\sqrt{2q\epsilon_{si}}}{C_{OX}} \sqrt{n_0 \phi_t \left[\exp\left(\frac{\Psi_s}{\phi_t}\right) - 1 \right]} \quad (6)$$

Numerical simulation results show this asymptotic approximation is accurately available for various traps states density. As shown in Fig. 1, in the subthreshold region, since an exponential DOS strongly affects its characteristics and most of the induced charge is trapped in deep states, surface potential can be approximately determined by Eq. (5). On the other hand, in strong inversion, when all the additional induced charge is free charge, the free charge dominates Poisson's equation, Eq. (1). Similar to MOSFET devices, surface potential can be approximated by Eq. (6).

We restrict our analysis to the strong inversion region. In this case, the exponential term in Eq. (6) becomes dominant, thereby reducing Eq. (6) to

$$V_g - V_{fb} - \Psi_s = \frac{\sqrt{2q\epsilon_{si} n_0 \phi_t}}{C_{OX}} \exp\left(\frac{\Psi_s}{2\phi_t}\right) \quad (7)$$

Equation (7) can be rearranged as

$$\frac{V_g - V_{fb} - \Psi_s}{2\phi_t} \exp\left(\frac{V_g - V_{fb} - \Psi_s}{2\phi_t}\right) = \frac{\sqrt{q\epsilon_{si}n_0}}{C_{OX}\sqrt{2\phi_t}} \exp\left(\frac{V_g - V_{fb}}{2\phi_t}\right) \quad (8)$$

Equation (8) can be accurately solved using the Lambert W function^[12], where $W_0(x)$ is the solution of the transcendental equation $W_0(x) \times \exp[W_0(x)] = x$. The Lambert W function has previously been used in many semiconductor device physics solutions and is also available in some circuit simulation tools.

The accurate and explicit expression for surface potential in the strong inversion region as a function of gate voltage is achieved by

$$\Psi_s = V_g - V_{fb} - 2\phi_t W_0 \left[\frac{\sqrt{q\epsilon_{si}n_0}}{C_{OX}\sqrt{2\phi_t}} \exp\left(\frac{V_g - V_{fb}}{2\phi_t}\right) \right] \quad (9)$$

Following the analogous derivation of Eq. (4), the electric field E in the vertical direction becomes

$$E(\Psi) = \frac{d\Psi}{dx} \approx \sqrt{\frac{2q}{\epsilon_{si}}} \left[n_i \phi_t \exp\left(\frac{E_{F0}/q}{\phi_t}\right) \exp\left(\frac{\Psi - \phi_n}{\phi_t}\right) + N_{TA00} \frac{E_1}{q} \exp\left(\frac{\Psi - \phi_n}{E_1/q}\right) \right]^{1/2} \quad (10)$$

where we have ignored the “-1” term because, in strong inversion, the exponential term of electrostatic potential is much larger than one, and N_{TA00}

$$= g_{cl} \frac{\pi kT}{\sin(\pi kT/E_1)} \exp\left(\frac{E_{F0} - E_C}{E_1}\right).$$

Applying the effective temperature approach^[13], an effective electric field E_{eff} is defined as

$$E_{eff}(\Psi) = A \exp\left(\frac{\Psi - \phi_n}{\phi_{eff}(\Psi)}\right) \quad (11)$$

where $A = \sqrt{\frac{2q}{\epsilon_{si}}} \left[n_i \phi_t \exp\left(\frac{E_{F0}/q}{\phi_t}\right) + N_{TA00} \frac{E_1}{q} \right]$, and

$\phi_{eff}(\Psi)$ is determined by $\phi_{eff}(\Psi) = \frac{\Psi - \phi_n}{\ln\left(\frac{E(\Psi)}{A}\right)}$ and

Eq. (10).

The induced free charge in the channel is given by

$$\begin{aligned} Q_i(\Psi_s) &= q \int_0^{\Psi_s} \frac{n(\Psi, \phi_n)}{d\Psi/dx} d\Psi \\ &= q \int_0^{\Psi_s} \frac{n(\Psi, \phi_n)}{E(\Psi)} d\Psi \approx q \int_0^{\Psi_s} \frac{n(\Psi, \phi_n)}{E_{eff}(\Psi)} d\Psi \end{aligned} \quad (12)$$

where $n(\Psi, \phi_n)$ is determined by Eq. (2).

Integrating Eq. (12) and using the relation in Eq. (7) yields

$$Q_i(\Psi_s) = qb_1 \left(\frac{V_g - V_{fb} - \Psi_s}{b_2} \right)^{2 - \frac{2\phi_t}{\phi_{eff}(\Psi_s)}} \quad (13)$$

where $b_1 = \frac{n_i \exp\left(\frac{E_{F0}/q}{\phi_t}\right)}{A} \times \frac{\phi_t \phi_{eff}(\Psi_s)}{\phi_{eff}(\Psi_s) - \phi_t}$, $b_2 = \frac{\sqrt{2q\epsilon_{si}\phi_t n_i}}{C_{OX}} \exp\left(\frac{E_{F0}/q}{2\phi_t}\right)$.

Hence, the free charge is now represented by Eq. (13), which depends on the surface potential. Under the assumption of gradual channel approximation, the poly-Si TFT drain current, which accounts for both the drift and diffusion components and is valid in both the linear and saturation regions, can be expressed as

$$I_{inv0} = \frac{W}{L} \mu_{eff} \left[\int_{\Psi_{s0}}^{\Psi_{sL}} Q_i(\Psi_s) d\Psi_s - \phi_t (Q_i(\Psi_{sL}) - Q_i(\Psi_{s0})) \right] \quad (14)$$

where Ψ_{s0} and Ψ_{sL} can be calculated using Eq. (9) by replacing ϕ_n with the applied source voltage V_s and the drain voltage V_d , respectively. The effective mobility model can be represented as

$$\mu_{eff} = \mu_s + \frac{\mu_0 \exp(-V_b/\phi_t)}{1 + \theta_1 (V_{gs})^{1/3} + \theta_2 (V_{gs})^2} \quad (15)$$

$$V_b = \left[(V_{gs} - V_i)^2 + (V_O - \kappa V_{ds})^2 \right]^{1/2} - (V_{gs} - V_i) \quad (16)$$

where μ_0 is the high field mobility, μ_s is the low field mobility, θ_1 and θ_2 are the mobility degradation parameters caused by phonon scattering and surface roughness scattering, respectively, V_O and V_i are the fitting potential barrier height parameters, and κ accounts for the potential barrier lowering effect induced by the drain. The above mobility parameters are extracted from the fitting between the model and data.

Substituting Eq. (13) into Eq. (14) and integrating, we find the drain current in the strong inversion region to be

$$I_{inv0} = \frac{W}{L} \mu_{eff} \left[g(\Psi_{sL}) - g(\Psi_{s0}) - \phi_t (Q_i(\Psi_{sL}) - Q_i(\Psi_{s0})) \right] \quad (17)$$

$$g(\Psi_s) = \frac{-qb_1}{(b_2)^{2 - \frac{2\phi_t}{\phi_{eff}(\Psi_s)}}} \times$$

$$\frac{\phi_{eff}(\Psi_s)}{3\phi_{eff}(\Psi_s) - 2\phi_t} \left[(V_g - V_{fb} - \Psi_s)^{3 - \frac{2\phi_t}{\phi_{eff}(\Psi_s)}} \right] \quad (18)$$

3 Subthreshold characteristics

In the subthreshold region, for moderate band-bending, most of the induced charge in poly-

Si TFTs resides in the localized states. The influence of trap states on the surface potential and drain current becomes dominant. As a consequence, surface potential in the subthreshold region is very well approximated by Eq. (5).

Around flat-band voltage, where off-state current is primarily determined by channel resistance, surface potential is smaller than or equal to a few E_1/q . Here, we restrict our analysis to gate bias above the flat-band voltage where the surface band bending is larger than a few E_1/q and the current-voltage characteristics are dominated by drift-diffusion. Therefore, neglecting the “-1” term, Equation (5) becomes

$$V_g - V_{fb} - \Psi_s = \frac{\sqrt{2q\epsilon_{si} N_{TA0} E_1/q}}{C_{OX}} \exp\left(\frac{\Psi_s}{2E_1/q}\right) \quad (19)$$

Applying the analogous derivation of Eq. (9), surface potential in the subthreshold region is solved analytically using the Lambert W function:

$$\Psi_s = V_g - V_{fb} - 2 \frac{E_1}{q} \times W_0 \left[\frac{\sqrt{q\epsilon_{si} N_{TA0}} \exp\left(\frac{V_g - V_{fb}}{2E_1/q}\right)}{C_{OX} \sqrt{2E_1/q}} \right] \quad (20)$$

Assuming that the contribution of the free carriers is negligible with respect to trapped ones, the electric field in the subthreshold region is evaluated by solving the Poisson's equation as

$$\frac{d\Psi}{dx} \approx \sqrt{\frac{2q}{\epsilon_{si}} N_{TA0} \frac{E_1}{q}} \exp\left(\frac{\Psi}{2E_1/q}\right) \quad (21)$$

For simplification, Equation (19) can be re-expressed as

$$\Psi_s - \phi_n = 2 \frac{E_1}{q} \ln \left[\frac{V_g - V_{fb} - \Psi_s}{b_3} \right] + \frac{E_C - E_{F0}}{q} \quad (22)$$

$$\text{where } b_3 = \frac{\sqrt{2q\epsilon_{si}}}{C_{OX}} \sqrt{g_{cl} \frac{E_1}{q} \times \frac{\pi kT}{\sin(\pi kT/E_1)}}.$$

As a result, from Eqs. (12), (21) and (22), the free charge in the channel can be written as

$$Q_i = q\eta \left(\frac{V_g - V_{fb} - \Psi_s}{b_3} \right)^{\frac{2E_1/q}{\phi_t} - 1} \quad (23)$$

$$\text{where } \eta = \frac{n_i}{\sqrt{\frac{2q}{\epsilon_{si}} \times \frac{E_1}{q} \times \frac{g_{cl} \pi kT}{\sin(\pi kT/E_1)}}} \times \frac{2\phi_t E_1}{2E_1 - q\phi_t} \times \exp\left(\frac{E_C}{q\phi_t}\right).$$

Again using Ohm's law and gradual channel approximation, the drain current of a poly-Si TFT

biased at the subthreshold region is expressed as

$$I_{\text{sub0}} = \frac{W}{L} \mu_{\text{eff}} \int_0^{V_{ds}} Q_i d\phi_n = \frac{W}{L} \mu_{\text{eff}} \int_{\Psi_{ss}}^{\Psi_{sd}} \frac{Q_i(\Psi_s)}{d\Psi_s/d\phi_n} d\Psi_s \quad (24)$$

where Ψ_{ss} and Ψ_{sd} can be calculated using Eq. (20) by replacing ϕ_n with the applied V_s and V_d , respectively.

Differentiating Eq. (19) with respect to Ψ_s and using Eq. (22), we obtain

$$\frac{d\phi_n}{d\Psi_s} = 1 + \frac{2E_1/q}{V_g - V_{fb} - \Psi_s} \quad (25)$$

Substituting Eqs. (23) and (25) into Eq. (24), the drain current for the subthreshold region can be derived as

$$I_{\text{sub0}} = - \frac{q\mu_{\text{eff}} W \eta}{L (b_3)^{\frac{2E_1/q}{\phi_t} - 1}} [f(\Psi_{sd}) - f(\Psi_{ss})] \quad (26)$$

$$f(\Psi_s) = \frac{\phi_t}{2E_1/q} (V_g - V_{fb} - \Psi_s)^{\frac{2E_1/q}{\phi_t} + 1} + 2 \frac{E_1}{q} \times \frac{\phi_t}{2E_1/q - \phi_t} (V_g - V_{fb} - \Psi_s)^{\frac{2E_1/q}{\phi_t} - 1} \quad (27)$$

So far we have obtained the drain current in the subthreshold and strong inversion region, which depends on the surface potential at the source end and drain end. The surface potential calculated in this paper needs no iterative procedures, and Eq. (9) for strong inversion and Eq. (20) for the subthreshold region are good approximations.

4 Kink effect

When the poly-Si TFTs are biased at high drain voltage, anomalous increasing drain current in saturation and a steeper subthreshold slope have been observed. These phenomena can be explained by the kink effect, which is much more pronounced in poly-Si TFTs. Impact ionization occurs in the high electric field region at the drain end of the channel. Similar to the floating body effect in SOI devices, the holes generated by impact ionization are injected into the floating body and reduce the potential barrier between the source and body, forcing additional electrons to be injected from the source. The extra injected electrons enter the high electric field region, where they are further amplified by impact ionization and collected by the drain. This floating body effect can be represented by a parasitic bipolar transistor (PBT) in parallel with the device.

In the subthreshold, the kink effect is reflected as a decreasing subthreshold swing for high drain voltage. This effect is modeled by impact ionization, and is not necessarily related to the activation of the PBT, because the PBT current gain β is very small in the subthreshold^[14]. Using the derivation in Ref. [15] leads to the following subthreshold current expression, including impact ionization:

$$I_{\text{sub}} = \left[1 + A_{\text{isub}} V_{\text{ds}} \exp\left(-\frac{B_{\text{isub}}}{V_{\text{ds}}}\right) \right] I_{\text{sub0}} \quad (28)$$

where A_{isub} and B_{isub} are the process-dependent fitting parameters.

In strong inversion, the modeled multiplication factor M tends to a similar expression as that used in Ref. [15], but the surface potential expression is adopted to release M from smoothing functions, which makes M negligible in the triode region. Therefore, it yields

$$M = A_i \left[V_{\text{ds}} - (\Psi_{\text{skink}} - \Psi_{\text{s0}}) \right] \exp\left[\frac{-B_i}{V_{\text{ds}} - (\Psi_{\text{skink}} - \Psi_{\text{s0}})} \right] \quad (29)$$

where A_i and B_i are the process-dependent fitting parameters, and Ψ_{skink} is determined using Eq. (9), replacing ϕ_n with V_{kink} . Here V_{kink} is empirical, and it strongly depends on V_{gs} with $V_{\text{kink}} = \alpha_{\text{kink}} V_{\text{gs}}$, where α_{kink} is an empirical parameter.

In saturation, the high electric field in the pinch-off region leads to a conducting PBT. As a consequence, the PBT effect greatly affects kink in saturation^[16]. Therefore,

$$I_{\text{inv}} = \frac{M + 1}{1 - \beta M} I_{\text{inv0}} \quad (30)$$

where PBT current gain β is dependent on V_{gs} . Since when V_{gs} increases, β decreases^[17], we empirically model β with $\beta = \beta_0 - k_1 V_{\text{gse}}$, where k_1 is a fitting parameter and V_{gse} is an effective gate voltage with $V_{\text{gse}} = V_{\text{gs}} \left[1 + (V_{\text{gs}}/V_{\text{gsat}})^{m_2} \right]^{-1/m_2}$. Here m_2 and V_{gsat} are the adjustable parameters.

5 Generalized model

By combining the currents that account for each distribution, a smooth drain current model valid in a wide range of operation is obtained by

$$I_{\text{ds}} = I_{\text{off}} + \left[\frac{1}{1/(I_{\text{sub}})^m + 1/(I_{\text{inv}})^m} \right]^{1/m} \quad (31)$$

where parameter m determines how sharply I_{ds} changes from subthreshold to strong inversion, and I_{off} is the off-current in the vicinity of flat-

band voltage^[18]:

$$I_{\text{off}} = W t_{\text{film}} \frac{q^2}{kT} n_i \left(\frac{kT}{2m^* \pi} \right)^{\frac{1}{2}} \exp\left(\frac{-E_B}{kT}\right) \frac{V_{\text{ds}}}{L/L_g} \quad (32)$$

where t_{film} is the thickness of the film, m^* is the effective mass of the carrier, E_B is the grain boundary barrier height, and L_g is the grain size.

As the channel length decreases, the saturation voltage is smaller than the pinch-off voltage because of carrier velocity saturation. Therefore, drain voltage when calculating Ψ_{sL} in strong inversion should be replaced by an effective drain voltage V_{dse} . V_{dse} tends to V_{d} in the linear region and to saturation voltage V_{dsat} in saturation, which can be written as^[3]

$$V_{\text{dse}} = V_{\text{d}} \left[1 + \left(\frac{V_{\text{d}}}{V_{\text{dsat}}} \right)^{m_1} \right]^{-1/m_1} \quad (33)$$

where parameter m_1 controls the transition from V_{d} to V_{dsat} , with $V_{\text{dsat}} = \alpha_{\text{sat}} V_{\text{gs}}$, where α_{sat} is an adjustable parameter.

As the channel length is decreased, the mobility of poly-Si TFTs increases^[19] and the kink effect significantly increases. Accordingly, related parameters, such as V_i , μ_0 , A_{isub} , A_i , k_1 and α_{kink} , should scale with channel length. They have a similar form of dependency of L , which can be described as

$$P = P_0 + a \exp(-L/L_0) \quad (34)$$

where P represents the channel length dependent parameters, such as V_i , μ_0 , A_{isub} , A_i , k_1 and α_{kink} .

6 Results and discussion

Based on the explicit approximation for surface potential, drain current of poly-Si TFTs can be calculated from Eq. (31). To verify the proposed model, we compared it with available experimental data from different TFTs. The parameters of these TFTs used in simulation are listed in Table 1.

The first validation is achieved by comparing our model to experimental data with different channel lengths from Ref. [3]. In Figs. 2(a) and (b), we can see that the drain current of the device is perfectly predicted by the new model. As shown in Figs. 3(a) and (b), for short channel devices, the kink effect becomes significant. Figure 3(a) shows that the subthreshold behavior of the devices exhibits stronger dependence on drain

Table 1 Parameters for simulation

Symbol/unit	TFTs in Figs. 2 and 3 ^[3]	TFTs in Fig. 4 ^[20]
$W/\mu\text{m}$	50	20
$t_{\text{film}}/\mu\text{m}$	0.1	0.1
$L_g/\mu\text{m}$	0.2	0.12
$C_{\text{OX}}/(\text{F}/\text{cm}^2)$	3.51×10^{-8}	5×10^{-8}
$g_{\text{cl}}/(\text{cm}^{-3} \cdot \text{eV}^{-1})$	2×10^{18}	6×10^{19}
E_1/eV	0.161	0.1
E_{F0}/eV	0.11	0.01
V_{fb}/V	-1.15	0.5
E_{B}/eV	0.11	0.01
$\mu_{\text{S}}/(\text{cm}^2/(\text{V} \cdot \text{s}))$	10	3
$\mu_{\text{D}}/(\text{cm}^2/(\text{V} \cdot \text{s}))$	$300 + \exp(-L)$	$18 + 103.5 \times \exp(-L/6)$
$\theta_1/\text{V}^{-1/3}$	10^{-3}	5×10^{-4}
θ_2/V^{-2}	6×10^{-4}	5×10^{-5}
V_{Q}/V	0.65	0.84
V_i/V	$1 - \exp(-L/2.6)$	$9 - 13.3 \times \exp(-L/4.2)$
κ	0	0
$A_{\text{isub}}/\text{V}^{-1}$	$14.12 \times \exp(-L/17.42)$	$0.272 \times \exp(-L/4.55)$
B_{isub}/V	20	1
A_i/V^{-1}	$0.026 \times \exp(-L/21.16)$	$0.073 \times \exp(-L/10)$
B_i/V	0.4	1
α_{kink}	$0.85 - \exp(-L/2)$	$0.85 - 0.6 \times \exp(-L/7.2)$
β_0	8.5	4.05
k_1/V^{-1}	$0.93 \times \exp(-L/27.34)$	$0.22 \times \exp(-L/18)$
m	1	1
$m_1 \ \& \ m_2$	4	4
V_{gsat}/V	25	22
α_{sat}	0.7	0.45

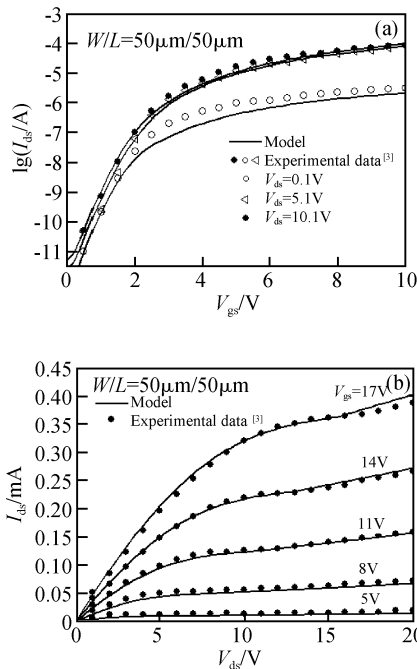


Fig. 2 Comparison of drain currents simulated from the proposed model with experimental data^[3] (a) I_{ds} versus V_{gs} with $W/L = 50\mu\text{m}/50\mu\text{m}$; (b) I_{ds} versus V_{ds} with $W/L = 50\mu\text{m}/50\mu\text{m}$

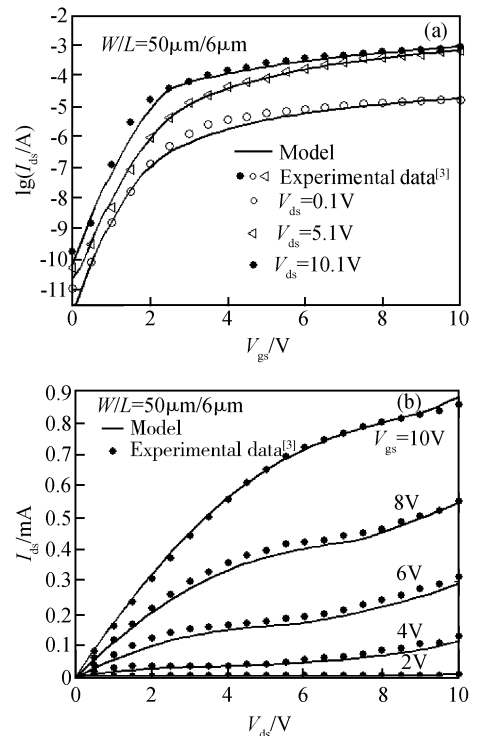


Fig. 3 Comparison of drain currents simulated from the proposed model with experimental data^[3] (a) I_{ds} versus V_{gs} with $W/L = 50\mu\text{m}/6\mu\text{m}$; (b) I_{ds} versus V_{ds} with $W/L = 50\mu\text{m}/6\mu\text{m}$

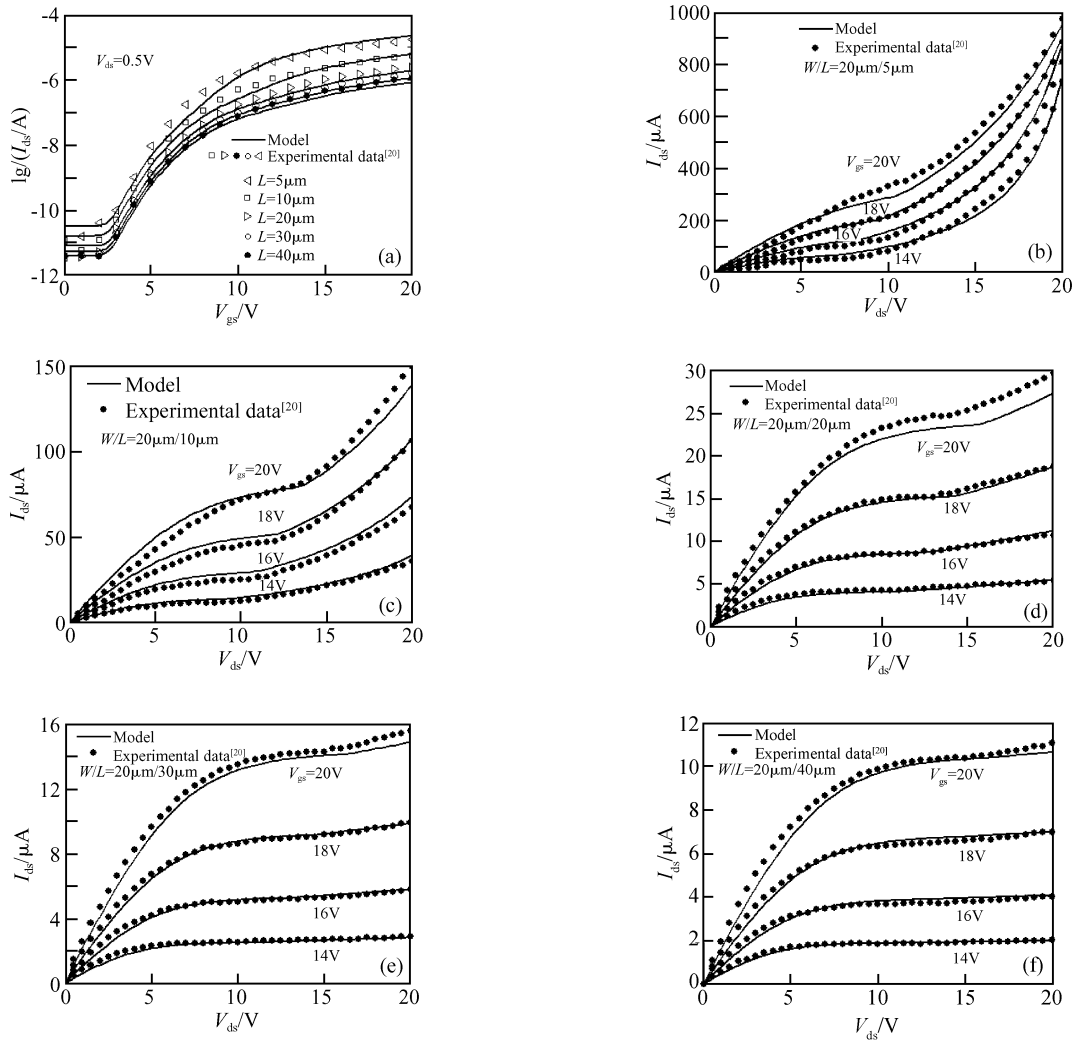


Fig. 4 Comparison of drain currents simulated from the proposed model with experimental data^[20] (a) I_{ds} versus V_{gs} ; (b) I_{ds} versus V_{ds} with $W/L = 20\mu\text{m}/5\mu\text{m}$; (c) I_{ds} versus V_{ds} with $W/L = 20\mu\text{m}/10\mu\text{m}$; (d) I_{ds} versus V_{ds} with $W/L = 20\mu\text{m}/20\mu\text{m}$; (e) I_{ds} versus V_{ds} with $W/L = 20\mu\text{m}/30\mu\text{m}$; (f) I_{ds} versus V_{ds} with $W/L = 20\mu\text{m}/40\mu\text{m}$

voltage. Meanwhile, output characteristics in Fig. 3(b) show that the current keeps rising after saturation due to the kink effect. Encouraging agreement is achieved for both long and short channel devices.

The second validation of the derived model is employed by a comparison to the experimental data from Ref. [20]. The devices were fabricated through the same process but with different channel lengths. Figure 4 indicates that, over a wide range of gate and drain voltages, the model is very close to the experimental data for both long and short channels. The kink effect is more pronounced in short-channel devices, and, at higher drain voltage, premature breakdown will occur.

7 Conclusions

In this paper, a new physical-based DC model for poly-Si TFTs valid in a wide range of channel lengths and operational regions has been presented. Our model has distinctive features. First, the proposed model accounts for a V-shaped exponential distribution of DOS. Second, the analytical approximation for the surface potential is derived, and the explicit calculation leads to a noticeable decrease in simulation time. Third, a complete drain current expression is deduced and can be easily implemented into circuit simulators. Fourth, the model accounts for the kink effect, which is important in subthreshold and satura-

tion. Fifth, the same model parameters but channel length L are used to model experimental data with different lengths, and good agreement is achieved.

References

- [1] Lin P, Guo J, Wu C. A quasi-two-dimensional analytical model for the turn-on characteristics of polysilicon thin-film transistors. *IEEE Trans Electron Devices*, 1990, 37: 666
- [2] Siddiqui M J, Qureshi S. Surface-potential-based charge sheet model for the polysilicon thin film transistors without considering kink effect. *Microelectronics Journal*, 2001, 32: 235
- [3] Jacunski M D, Shur M S, Owusu A A, et al. A short-channel DC SPICE model for polysilicon thin-film transistors including temperature effects. *IEEE Trans Electron Devices*, 1999, 46: 1146
- [4] Chung S S, Chen D C, Cheng C T, et al. A physically-based built-in spice poly-Si TFT model for circuit simulation and reliability evaluation. *Proc of the IEEE International Electron Devices Meeting, San Francisco*, 1996: 139
- [5] Li C C, Ikeda H, Inoue T, et al. A physical poly-silicon thin film transistors model for circuit simulations. *Proc of the IEEE International Electron Devices Meeting, Washington*, 1993: 497
- [6] Werner J, Peisl M. Exponential band tails in polycrystalline semiconductor films. *Phys Rev B*, 1985, 31: 6881
- [7] Fortunato G, Migliorato P. Determination of gap state density in polycrystalline silicon by field-effect conductance. *Appl Phys Lett*, 1986, 49: 1025
- [8] Chen S S, Shone F C, Kuo J B. A closed-form inversion-type polysilicon thin-film transistor DC/AC model considering the kink effect. *J Appl Phys*, 1995, 77: 1776
- [9] Fortunato G, Migliorato P. Model for the above-threshold characteristics and threshold voltage in polycrystalline silicon transistors. *J Appl Phys*, 1990, 68: 2463
- [10] Ono K, Aoyama T, Konishi N, et al. Analysis of current-voltage characteristics of low-temperature-processed polysilicon thin-film transistors. *IEEE Trans Electron Devices*, 1992, 39: 792
- [11] Fortunato G, Meakin D B, Migliorato P. The sub-threshold characteristics of polysilicon thin-film-transistors. *Jpn J Appl Phys*, 1988, 27: 2124
- [12] Corless R M, Gonnet G H, Hare D E G, et al. On Lambert's W function. *Adv Comput Math*, 1996, 5: 329
- [13] Chen S S, Kuo J B. An analytical a-Si: H TFT DC/capacitance model using an effective temperature approach for deriving a switching time model for an inverter circuit considering deep and tail states. *IEEE Trans Electron Devices*, 1994, 41: 1169
- [14] Jenö T, Heinrich S. Properties of ESFI MOS transistors due to the floating substrate and the finite volume. *IEEE Trans Electron Devices*, 1975, 22: 1017
- [15] Iñiguez B, Fjeldly T A. Unified substrate current model for MOSFETs. *Solid-State Electron*, 1997, 41: 87
- [16] Valletta A, Gaucci P, Mariucci L, et al. Modelling velocity saturation and kink effects in p-channel polysilicon thin-film transistors. *Thin Solid Films*, 2007, 515: 7417
- [17] Valdinoci M, Colalongo L, Baccarani G, et al. Floating body effects in polysilicon thin-film transistors. *IEEE Trans Electron Devices*, 1997, 44: 2234
- [18] Baccarani G, Ricco B. Transport properties of polycrystalline silicon films. *J Appl Phys*, 1978, 49: 5565
- [19] Ng K K, Celler G K, Povilonis E I, et al. Effects of grain boundaries on laser crystallized poly-Si MOSFET's. *IEEE Trans Electron Device Lett*, 1981, 2(12): 316
- [20] Chen H L, Wu C Y. A new $I-V$ model considering the impact-ionization effect initiated by the DIGBL current for the intrinsic n-channel poly-Si TFT's. *IEEE Trans Electron Devices*, 1999, 46: 722

用于器件描述和电路仿真的新型多晶硅 TFT 直流模型*

邓婉玲[†] 郑学仁 陈荣盛

(华南理工大学微电子研究所, 广州 510640)

摘要: 提出一种新型的多晶硅薄膜晶体管电流-电压物理模型. 考虑了陷阱态密度的 V 形指数分布, 运用 Lambert W 函数推出了表面势的显式求解方法, 大大提高了运算效率, 在电路仿真中发挥了重要作用. 基于指数的陷阱态密度和计算的表面势, 描述了亚阈值区和强反型区的漏电流特性. 推导了完整、统一的漏电流表达式, 包括翘曲效应. 在很广的沟道长度范围和工作区内, 模型和实验数据一致.

关键词: 多晶硅薄膜晶体管; 表面势; 直流模型; 翘曲效应

EEACC: 2560B **PACC:** 7340N

中图分类号: TN321 **文献标识码:** A **文章编号:** 0253-4177(2007)12-1916-08

* Cadence 设计系统公司资助项目

[†] 通信作者, Email: dwanl@126.com

2007-07-21 收到, 2007-08-30 定稿